

# Efimov States of Strongly Interacting Photons

M. J. Gullans,<sup>1,2,\*</sup> S. Diehl,<sup>3</sup> S. T. Rittenhouse,<sup>4</sup> B. P. Ruzic,<sup>1</sup> J. P. D’Incao,<sup>5,6</sup> P. Julienne,<sup>1</sup> A. V. Gorshkov,<sup>1,2,†</sup> and J. M. Taylor<sup>1,2,7,‡</sup>

<sup>1</sup>*Joint Quantum Institute, NIST and University of Maryland, College Park, Maryland 20742, USA*

<sup>2</sup>*Joint Center for Quantum Information and Computer Science,  
NIST and University of Maryland, College Park, Maryland 20742, USA*

<sup>3</sup>*Institut für Theoretische Physik, Universität zu Köln, D-50937 Cologne, Germany*

<sup>4</sup>*Department of Physics, The United States Naval Academy, Annapolis, Maryland 21402, USA*

<sup>5</sup>*JILA, University of Colorado and NIST, Boulder, Colorado 80309, USA*

<sup>6</sup>*Department of Physics, University of Colorado, Boulder, Colorado 80309, USA*

<sup>7</sup>*Research Center for Advanced Science and Technology (RCAST),  
The University of Tokyo, Meguro-ku, Tokyo, 153-8904, Japan*

(Dated: December 14, 2024)

We demonstrate the emergence of universal Efimov physics for interacting photons in cold gases of Rydberg atoms. We consider the behavior of three photons injected into the gas in their propagating frame, where a paraxial approximation allows us to consider them as massive particles. In contrast to atoms and nuclei, the photons have a large anisotropy between their longitudinal mass, arising from dispersion, and their transverse mass, arising from diffraction. Nevertheless, we show that in suitably rescaled coordinates the effective interactions become dominated by  $s$ -wave scattering near threshold and, as a result, give rise to an Efimov effect near unitarity, but with spatially anisotropic wavefunctions in the original coordinates. We show that the three-body loss of these Efimov trimers can be strongly suppressed and determine conditions under which these states are observable in current experiments. These effects can be naturally extended to probe few-body universality beyond three bodies, as well as the role of Efimov physics in the non-equilibrium, many-body regime.

The problem of classifying the universal properties of few-body systems near unitarity, i.e., a divergence in the two-body scattering length  $a$ , was first undertaken for the three-body problem by Vitaly Efimov in 1970, who discovered an infinite series of three-body bound states obeying a geometrical scaling relation [1]. This discovery served as an important guide to theoretical work in few-body physics in subsequent years [2], but the observation of such Efimov trimers in nature remained elusive until pioneering experiments on cold atomic gases reported direct signatures of these states in atomic loss spectroscopy [3]. That success reinvigorated work on the classification problem alluded to above, including in systems other than cold atoms [4, 5]. As a result, recent years have seen the elucidation of many universal properties of  $N$ -body systems for  $N \geq 3$  [6–13], including the many-body, short-time dynamics of Efimov trimers in a unitary Bose gas [14]. Despite this progress, Efimov states, as well as larger bound state clusters, are typically associated with large inelastic losses in cold atom systems due to strong three-body recombination. These losses generally preclude the study of many-body physics of Efimov trimers (e.g., the formation of a Bose-Einstein condensate of trimers [15]), and limit efforts to study universal bound states for large  $N$ .

Recently, it has become possible to achieve strong interactions between single photons by dressing light with strongly interacting Rydberg atoms to form Rydberg polaritons [16, 17]. The resulting photon-photon interactions have been used to study a diverse array of quantum nonlinear optical effects including: single-photon block-

ade and transistors [18–22], two-photon phase gates [23–25], and the formation of one dimensional few-photon bound states [26–30, 42]. Combining these strong interactions with the high degree of available control over the optical and atomic degrees of freedom makes these systems a promising platform for exploring non-equilibrium quantum many-body physics and realizing quantum simulation [31–39].

In this Letter, we show how such systems of interacting photons can lead to the formation of Efimov states of light. We analytically demonstrate that these Efimov states are spatially anisotropic due to the anisotropic mass of the polaritons and propagate in the medium as the three-body limit of an optical soliton. This property allows them to be distinguished from non-bound states in the system, which will dephase due to dispersive and diffractive effects [26, 29]. Unlike conventional cold atom systems, we find that the three-body losses can be strongly suppressed in this system, which allows for the formation of long-lived Efimov trimers. We consider the conditions under which these states can be directly observed in current experiments.

The basic configuration to realize interacting photons via atomic Rydberg states is shown in Fig. 1(a). The Rydberg atoms are dressed with a quantum field of light using electromagnetically induced transparency (EIT). Rydberg-Rydberg interactions lead to the Rydberg blockade effect [41], whereby a single atom (polariton) in the state  $|s\rangle$  shifts the  $s$ -state of nearby atoms out of resonance, leading to a strong optical nonlinearity. To describe the light transmission of this system, we in-

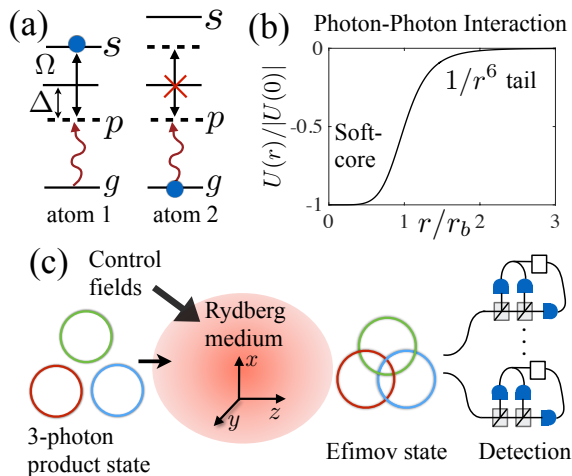


FIG. 1: (a) Schematic of EIT and the Rydberg blockade effect. (b) Effective interaction potential for the Rydberg polaritons. (c) The Efimov states emerge in transmission because, unlike non-bound three-body states, they are immune to dispersion and diffraction inside the medium. Spatially resolving multi-mode, three-photon coincidence measurements allow for detailed characterization of these states [29, 40].

roduce a bosonic field  $\psi(\mathbf{r})$  associated with the Rydberg dark-state polaritons. The bare interaction between the Rydberg atoms is given by the van der Waals interaction  $V(\mathbf{r}) = -C_6/r^6$ , however, the effective interactions between polaritons take the form [see Fig. 1(b)] [42]

$$U(\mathbf{r}) = \frac{\alpha V(\mathbf{r})}{1 - \bar{\chi}V(\mathbf{r})}, \quad (1)$$

where  $\bar{\chi}$  and  $\alpha$  are a function of the control parameters and atomic decay rates [43]. Here we consider the case  $\bar{\chi}, C_6 > 0$  with a large detuning from the intermediate state so that  $U(\mathbf{r})$  is attractive, non-singular, and conservative.  $U(\mathbf{r})$  has a long range van der Waals tail, but saturates to a constant value for  $r \ll r_b$ , where the blockade radius is defined as  $r_b = |\bar{\chi}C_6|^{1/6}$ . Using these effective interactions we can describe the few-body propagation of Rydberg polaritons by the second-quantized Hamiltonian density

$$\mathcal{H} = \psi^\dagger(\mathbf{r}) \left[ -i\hbar v_g \partial_z - \frac{\hbar^2 \partial_z^2}{2m_z} - \frac{\hbar^2 \partial_\perp^2}{2m_\perp} \right] \psi(\mathbf{r}) + \int d^3 r' \psi^\dagger(\mathbf{r}) \psi^\dagger(\mathbf{r}') U(\mathbf{r} - \mathbf{r}') \psi(\mathbf{r}') \psi(\mathbf{r}), \quad (2)$$

where  $v_g$  is the EIT group velocity,  $m_z$  is the longitudinal mass arising from dispersive effects,  $m_\perp$  is the transverse mass arising from diffraction in the paraxial wave approximation, and  $\partial_\perp^2 = \partial_x^2 + \partial_y^2$ . The lowest order correction to this model is a short-range, three-body force [27–30], however, we neglect this short-range force here as it is expected to play a minor role in the Efimov physics when the two-body interaction potential has a  $1/r^6$  tail [44–46].

After transforming into a co-moving frame, apart from the anisotropic mass, this model has a standard form studied in few-body atomic and nuclear systems. Furthermore, near threshold, we find that the anisotropy in the mass can be accounted for by a simple rescaling of the coordinates and the scattering becomes effectively isotropic in the absence of higher partial wave resonances. This implies that the universal few-body hierarchy, beginning with the Efimov effect will arise near unitarity for such three-dimensional (3D) Rydberg polaritons.

The preparation and detection scheme for the Efimov states is illustrated in Fig. 1(c). The entrance into the medium acts as a quantum quench [26, 27], generating a finite overlap with the Efimov states. Once they are formed inside the medium, the bound states propagate without distortion, while the scattering states dephase with each other. As a result, for a sufficiently long medium in the absence of losses, the output will be dominated by the Efimov states. This effect has been used previously in 1D Rydberg polariton experiments to directly observe the formation of two and three-body bound states [26, 29]. When there is more than one bound state in the medium, these states are distinguishable by their spatial structure or propagation phase through the medium. To directly probe these states one can use time-resolved, three-photon coincidence measurements to access their longitudinal spatial structure, while multi-mode spatial resolution can probe their transverse structure [29, 40].

*Few-Body Scattering with Anisotropic Mass.*—To understand the origin of the non-interacting part of Eq. (2), we consider the Hamiltonian for a single polariton with total wavevector  $k = \sqrt{(k_0 + q_z)^2 + q_\perp^2}$  ( $\hbar = 1$ )

$$H = \begin{pmatrix} ck - ck_0 & g & 0 \\ g & \Delta & \Omega \\ 0 & \Omega & 0 \end{pmatrix}, \quad (3)$$

where  $\mathbf{q}$  is the momentum relative to  $k_0 \hat{z}$ ,  $g = \mu_{\text{at}} \sqrt{ck_0 n / \hbar \epsilon_0}$  is the single-photon Rabi frequency of the probe,  $\epsilon_0$  is the dielectric constant,  $n$  is the atomic density,  $\mu_{\text{at}}$  is the atomic dipole moment,  $\Omega$  is the control field Rabi frequency, and  $\Delta$  is the detuning between the control field and  $|p\rangle$  to  $|s\rangle$  transition frequency [see Fig. 1(a)]. We include the decay from the intermediate state by adding an imaginary component to  $\Delta \rightarrow \Delta - i\gamma$ , where  $\gamma$  is the halfwidth of the  $p$ -state. For every  $\mathbf{q}$ ,  $H$  has three eigenvalues  $\epsilon_\mu(\mathbf{q})$ , which can be used to find the group velocity and effective mass of the polaritons

$$v_g = \left. \frac{d\epsilon_{\mu^*}}{dq_z} \right|_{\mathbf{q}^*} = c \frac{[\Omega^2 + \omega(\Delta - \omega)]^2}{g^2(\Omega^2 + \omega^2)}, \quad (4)$$

$$\frac{1}{m_z} = \left. \frac{d^2 \epsilon_{\mu^*}}{dq_z^2} \right|_{\mathbf{q}^*} = \frac{2v_g^2}{\Omega^2 + \omega^2} \frac{\Omega^2(\Delta - 3\omega) - \omega^3}{\Omega^2 + \omega(\Delta - \omega)}, \quad (5)$$

$$\frac{1}{m_\perp} = \left. \frac{d^2 \epsilon_{\mu^*}}{dq_\perp^2} \right|_{\mathbf{q}^*} = \frac{v_g}{k_0}, \quad (6)$$

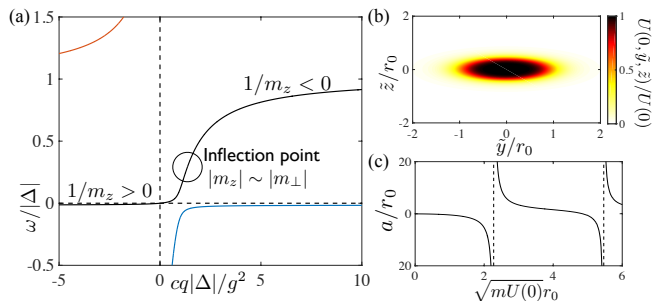


FIG. 2: (a) Dispersion relation near EIT resonance and inflection point for three polariton branches  $U$  (red),  $D$  (black), and  $L$  (blue). We took  $\Omega/2\pi = 5$  MHz,  $\Delta = 40$  MHz, and  $g/2\pi = 100$  MHz. Here  $g$  was taken to be smaller than its value in typical experiments to aid visibility. (b) Shape of potential in rescaled coordinates. (c) Scattering length as a function of the depth of the potential for  $m_{\perp}/m_z = 10$ . The first resonance occurs near  $\sqrt{mU(0)r_0} = 2.27$ .

where  $\epsilon_{\mu^*}(\mathbf{q}^*) = \omega$  is only satisfied for one choice of  $\mathbf{q}^*$  and  $\mu^* \in \{U, D, L\}$  [see Fig. 2(a)] and we take  $\mathbf{q}_{\perp}^* = 0$ . Here we have neglected higher order corrections in  $\Omega/g$ . From these expressions we see that, on EIT resonance ( $\omega = 0$ ), the mass ratio  $m_z/m_{\perp} = g^2/2c\Delta k_0 = (3\pi\gamma/\Delta)nk_0^{-3}$ .

More generally, the mass ratio can be independently tuned by taking advantage of the unconventional dispersion relation for the dark-state polaritons. This is illustrated in Fig. 2(a), which shows that the inverse longitudinal mass goes through a sign change for incoming probe frequencies away from the EIT resonance. From Eq. (5) we see that the inflection point occurs near  $\omega = (\Omega^2\Delta)^{1/3}$ . Operating near this inflection point allows one to equalize the mass ratio; however, it does not remove the effect of inelastic losses.

We define the average mass  $m^{-1} = (m_z^{-1} + m_{\perp}^{-1})/2$  and parametrize the mass ratio as  $\tan^2(\beta) = m_z/m_{\perp}$ . The condition to neglect the inelastic losses, which applies to both the EIT resonance and the inflection point in the limit  $\Delta \gg \gamma, |\omega|$ , is given by

$$\frac{\text{Re}(m^{-1})}{\text{Im}(m^{-1})} \approx \frac{3\pi}{2\beta^2} \frac{n}{k_0^3} \gg 1. \quad (7)$$

For example, for atomic densities near  $10^{13} \text{ cm}^{-3}$ ,  $\beta$  should be less than 0.1. It is also worth noting that the regime where  $\beta \approx 1$  and Eq. (7) predicts small inelastic losses precisely coincides with the regime of Dicke superradiance  $n/k_0^3 \gtrsim 1$  [47]. In this regime, our assumption of independent decay channels for the atomic radiation would have to be re-visited.

To understand the role of such a large anisotropy in the mass on the few-body scattering problem, we first consider the two-body problem with an anisotropic mass. The Schrödinger equation for two particles in the center

of mass frame takes the form

$$-\frac{1}{m}\tilde{\nabla}^2\psi + U(\tilde{\mathbf{r}})\psi = E\psi \quad (8)$$

where  $E$  is the energy and we have transformed to rescaled coordinates  $\tilde{z} = z/\sqrt{2}\cos\beta$  and  $(\tilde{x}, \tilde{y}) = (x, y)/\sqrt{2}\sin\beta$  such that the kinetic energy term becomes isotropic and the interactions become anisotropic [see Fig. 2(b)]. The characteristic length scale of the potential in the rescaled coordinates is given by  $r_0 = r_b/\sqrt{2}\sin\beta$ . In these rescaled coordinates we see that the interaction term mixes different two-body angular momentum  $\ell$  sectors.

We can represent the scattering amplitude as [48]

$$f(\hat{\mathbf{k}}_i, \hat{\mathbf{k}}_f) = -\frac{2\pi}{k} \sum_{\ell' \ell m} i^{\ell} Y_{\ell m}(\hat{\mathbf{k}}_f) T_{\ell \ell'}^{(m)} i^{-\ell'} Y_{\ell' m}^*(\hat{\mathbf{k}}_i), \quad (9)$$

where  $T = i(S - 1)$  is the transition matrix and  $\mathbf{k}_i$  and  $\mathbf{k}_f$  are the initial and final momentum states. For low-energies, the higher angular momentum channels are subject to a large centrifugal barrier, which allows the interactions to be treated perturbatively. In particular, for an interaction potential that falls off as  $1/r^{\delta}$  with  $\delta > 3$  and for  $\ell + \ell' \geq 2$ , the  $T$ -matrix elements scale as [48, 49]

$$|T_{\ell \ell'}^{(m)}| \sim \text{constant } k^{\ell + \ell' + 1} + \text{constant } k^{\delta - 2}. \quad (10)$$

We numerically verify these scalings near threshold for a large value of the mass ratio in the supplemental material [43]. These scalings suggest that the potential appears completely isotropic near threshold as all the partial waves with  $\ell, \ell' > 0$  are suppressed in the absence of higher-partial wave resonances. On the other hand, for the  $s$ -wave channel there is no centrifugal barrier and, even near threshold, the non-perturbative corrections to Eq. (10) are important. To tune near unitarity in this system we take advantage of shape resonances in the  $s$ -wave scattering length. In Fig. 2(c) we show the positions of the first two scattering resonances as a function of the depth of the potential  $\sqrt{mU(0)r_0}$ , which can be tuned via  $\Omega$  or  $\Delta$ .

These features of the two-body problem have important implications for the three-body problem as well. In particular, this analysis directly implies that the three-body hyperspherical potential  $U_3(R)$  will have the universal behavior in the region  $r_0 \ll R \ll a$  [1, 2]

$$-\frac{\sqrt{3}}{2m} \left[ \frac{d^2}{dR^2} + \frac{s_0^2 + 1/4}{R^2} \right] f_n(R) = E_n f_n(R) \quad (11)$$

where  $s_0 = 1.00624$ ,  $R$  is the three-body hyperradius in the rescaled coordinates [43], and  $f_n$  is the hyperradial component of the three-body wavefunction in hyperspherical coordinates. For distances on the order of  $r_0$  this equation is no longer accurate as the character of the two-body interactions [Eq. (1)] become important.

However in the region,  $R \ll r_b$  we can also find the hyperspherical potential analytically because the two-body potential approaches a constant and

$$-\frac{\sqrt{3}}{2m} \left[ \frac{d^2}{dR^2} - \frac{15/4}{R^2} \right] f_n(R) = [E_n - 3U(0)]f_n(R), \quad (12)$$

which has a repulsive centrifugal barrier. To better understand the intermediate region  $r_b \lesssim R \lesssim r_0$ , we have performed numerical calculations [50, 51] of  $U_3(R)$  that include the coupling to higher-partial waves as a perturbative correction to the two-body  $s$ -wave potential [43]. The results are shown in Fig. 3(a) for the first scattering resonance with  $m_\perp/m_z = 10$ . We see good agreement with the two analytic predictions in the small and large  $R$  limits. The presence of the long-range  $1/R^2$  potential near unitarity shows that the three-body problem will give rise to an Efimov effect with an infinite series of three-body bound states, with energies ( $n = 0, 1, \dots$ )

$$E_n = -\frac{\kappa_*^2}{m} e^{-2\pi n/s_0}, \quad (13)$$

while the presence of the centrifugal barrier near  $R \sim r_0$  suggests the scaling for the three-body parameter  $\kappa_* \sim 1/r_0$  [44, 46, 52].

*Suppression of Three-Body Loss.*—In cold-atom systems, the lifetime of the Efimov states is limited by their decay into deeply bound two-body states. In this Rydberg polariton system we can avoid such effects by tuning the system near the first scattering resonance in Fig. 2(c), where no deep two-body bound states exist. We can also avoid inelastic two-body loss by going to sufficiently large detunings  $\Delta$ . However, due to the multi-component nature of the polariton system and the unconventional dispersion relations, three-body loss processes are still allowed whereby energy and momentum is conserved by scattering the polaritons far away from their initial momentum. As shown in Fig. 3(b), near the inflection point, two such three-body loss processes are allowed. In one case, one of the polaritons has a final state on the lower polariton branch, while, in the other case, all three polaritons end on the dark-state branch. On EIT resonance, energy and momentum conservation only allow the former process.

Despite the presence of these additional loss channels, we find that their contribution to the three-body loss is strongly suppressed because the Rydberg blockade mechanism leads to an exponentially small two-body potential for large relative momenta  $\delta q \gg r_b^{-1}$ . In particular, for the three-body loss channels in Fig. 3(b) each process involves a finite momentum transfer  $\delta q$ . When the minimum  $\delta q \gg r_b^{-1}$ , we can estimate the three-body loss rate perturbatively in the Fourier transform of  $U(r)$

$$U_{\mathbf{q}} = -\frac{4\pi^2\alpha r_b^2}{3q\bar{\chi}} \left[ e^{-qr_b} - 2\text{Re} \left( e^{-qr_b e^{i\pi/3} - i\pi/3} \right) \right]. \quad (14)$$

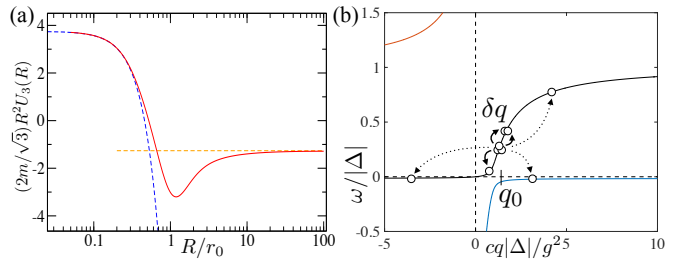


FIG. 3: (a) (red) Rescaled three-body hyperspherical potential at the first scattering resonance for  $m_\perp/m_z = 10$ . (yellow) In the region  $R \gg r_0$ ,  $U_3(R)$  approaches the universal form that gives rise to the Efimov effect. (blue) Analytic result in the region  $R \ll r_b$ . (b) Three-body loss processes near inflection point (same branch and different branch, see text), where  $q_0$  is the incoming momentum of the polaritons.

From which we see that the three-body loss channels will be exponentially suppressed as  $e^{-\delta q r_b}$ . Near the inflection point, the minimum  $\delta q$  (and thus the dominant channel) occurs for the process where all three polaritons end on the dark-state branch, which we can find analytically by expanding the dispersion to third order around the momentum of the polaritons  $\mathbf{q}_0$

$$\epsilon_D(q) = \epsilon_D(q_0) + v_g \delta q_z + \frac{\delta q_z^2}{2m_z} + \frac{\delta q_\perp^2}{2m_\perp} + \frac{\eta \delta q_z^3}{6}, \quad (15)$$

where  $\eta = d^3 \epsilon_D / d^3 q_z |_{q_0}$ . The three-body resonance condition  $3\epsilon_D(\mathbf{q}_0) = 2\epsilon_D(\mathbf{q}_0 + \delta \mathbf{q}) + \epsilon_D(\mathbf{q}_0 - 2\delta \mathbf{q})$  has a minimum  $|\delta \mathbf{q}|$  when  $\delta q_\perp = 0$  and  $\delta q_z = 3/\eta m_z$ . Thus, three-body losses will be suppressed when

$$\delta q_z r_b \approx \left( \frac{g^2}{ck_0 \Delta} \right)^{5/3} (r_b k_0)^{1/3} \frac{\Phi^{2/3}}{\beta^3} \gg 1, \quad (16)$$

where the value of  $\Phi \equiv \sqrt{mU(0)}r_0$  is determined by the position of the first scattering resonance [e.g., see Fig. 2(c)]. In the supplemental material we give the full scaling of the three-body loss parameter [43]. For a density of  $10^{13} \text{ cm}^{-3}$  with a blockade radius of  $20 \mu\text{m}$  [26], this implies that  $\beta$  should be less than 0.1 to strongly suppress the three-body losses.

On EIT resonance, the minimum  $\delta q \approx g^2/c\Delta$  and the condition to neglect three-body loss is simply that  $\phi \gg 1$ . This scaling implies that three-body loss will still play an important role near the first scattering resonance because, on EIT resonance,  $\Phi \approx \phi$ . Thus we see the primary advantage of working near the inflection point is the control it provides over the mass ratio, scattering length, and three-body loss rate.

*Preparation and Detection.*—To prepare the Efimov states we propose to use the high-degree of control over the two-body parameters to tune the scattering length ( $a < 0$ ) to values in which the trimers cross zero energy. As each such value is crossed in the space of control

parameters, an Efimov state will emerge in transmission through the medium due to the quench dynamics described in the introduction. When more than one Efimov state is present in the medium, they can be distinguished from each other by changing the transverse focus of the input field to increase the initial overlap with the desired state.

The two primary experimental requirements to realize such long-lived Efimov trimers are given by Eq. (7) and Eq. (16). A third important consideration is that the size of the Efimov state does not exceed the size of the atomic cloud. This is of particular relevance for small values of  $\beta$  because, when the coordinates are transformed back to the lab-coordinates, we see that the longitudinal size of the Efimov states will scale as  $r_0 \approx r_b/\beta$ . For an atomic density of  $10^{13} \text{ cm}^{-3}$ , we require  $\beta < 0.1$ , which implies that the length of the atomic cloud should be greater than  $100 \text{ }\mu\text{m}$ . The condition to observe the second Efimov trimer is more demanding as this state is a factor of 22.7 times larger. However, this scale factor can be reduced by using mixed species systems with differing mass ratios [53], which is achievable in our system by using multi-color input fields.

*Conclusions.*—We have demonstrated that systems of interacting photons formed from Rydberg polaritons naturally give rise to an Efimov effect. A distinct advantage of this system is that one can realize long-lived Efimov trimers by tuning the system to the first scattering resonance and suppressing other three-body loss channels. The wide range of control over the system parameters and the absence of  $N$ -body losses make this a promising platform for studying few-body universality. At the same time, increasing the input light intensity provides access to the non-equilibrium, many-body regime where the role of universal few-body physics is poorly understood. The resulting photonic states that emerge from the medium have a rich multi-particle entanglement structure, which may enable them to be used as a resource for optics-based quantum technologies [40, 54].

*Acknowledgements.*— We acknowledge helpful discussions with W. D. Phillips, T. Porto, H. P. Büchler, P. Zoller, M. D. Lukin, V. Vuletic, and Q.-Y. Liang. MJG and SD would like to thank the organizers of the workshop on “Quantum Simulation and Many-Body Physics with Light” in Crete, Greece where some of this work was completed. This research was supported by the European Research Council through Grant Agreement No. 647434 (DOQS), NSF through Grant No. PHY-1607204, ARL CDQI, NSF QIS, AFOSR, ARO, ARO MURI, and the NSF-funded Physics Frontier Center at the JQI.

lans@princeton.edu

† gorshkov@umd.edu

‡ jmtaylor@jqi.umd.edu

- [1] V. N. Efimov, *Sov. J. Nucl. Phys.* **12**, 589 (1971); *Phys. Rev. C* **47**, 1876 (1993).
- [2] E. Braaten and H. W. Hammer, *Universality in few-body systems with large scattering length*, *Phys. Rep.* **428**, 259 (2006).
- [3] T. Kraemer, M. Mark, P. Waldburger, J. G. Danzl, C. Chin, B. Engeser, A. D. Lange, K. Pilch, A. Jaakkola, H. C. Nägerl, et al., *Evidence for Efimov quantum states in an ultracold gas of caesium atoms*, *Nature* **440**, 315 (2006).
- [4] Y. Nishida, Y. Kato, and C. D. Batista, *Efimov effect in quantum magnets*, *Nature Phys.* **9**, 93 (2013).
- [5] M. Kunitski, S. Zeller, J. Voigtsberger, A. Kalinin, L. P. H. Schmidt, M. Schoffler, A. Czasch, W. Scholkopf, R. E. Grisenti, T. Jahnke, et al., *Observation of the Efimov state of the helium trimer*, *Science* **348**, 551 (2015).
- [6] L. Platter, H.-W. Hammer, and U.-G. Meißner, *Four-boson system with short-range interactions*, *Phys. Rev. A* **70**, 052101 (2004).
- [7] H. W. Hammer and L. Platter, *Universal properties of the four-body system with large scattering length*, *Eur. Phys. J. A* **32**, 113 (2007).
- [8] F. Ferlaino, S. Knoop, M. Berninger, W. Harm, J. P. D’Incao, H.-C. Nägerl, and R. Grimm, *Evidence for universal four-body states tied to an efimov trimer*, *Phys. Rev. Lett.* **102**, 140401 (2009).
- [9] J. von Stecher, J. P. D’Incao, and C. H. Greene, *Signatures of universal four-body phenomena and their relation to the Efimov effect*, *Nature Phys.* **5**, 417 (2009).
- [10] N. Mehta, S. Rittenhouse, J. D’Incao, J. von Stecher, and C. Greene, *General Theoretical Description of  $N$ -Body Recombination*, *Phys. Rev. Lett.* **103**, 153201 (2009).
- [11] R. Schmidt and S. Moroz, *Renormalization-group study of the four-body problem*, *Phys. Rev. A* **81**, 052709 (2010).
- [12] A. Zenesini, B. Huang, M. Berninger, S. Besler, H.-C. Ngerl, F. Ferlaino, R. Grimm, C. H. Greene, and J. von Stecher, *Resonant five-body recombination in an ultracold gas of bosonic atoms*, *New J. Phys.* **15**, 043040 (2013).
- [13] C. H. Greene, P. Giannakeas, and J. Perez-Rios, *Universal few-body physics and cluster formation*, arXiv:1704.02029 (2017).
- [14] C. E. Klauss, X. Xie, C. Lopez-Abadia, J. P. D’Incao, Z. Hadzibabic, D. S. Jin, and E. A. Cornell, *Observation of Efimov molecules created from a resonantly interacting Bose gas*, arXiv:1704.01206 (2017).
- [15] E. Braaten, H. W. Hammer, and M. Kusunoki, *Efimov States in a Bose-Einstein Condensate near a Feshbach Resonance*, *Phys. Rev. Lett.* **90**, 170402 (2003).
- [16] J. D. Pritchard, D. Maxwell, A. Gauguier, K. J. Weatherill, M. P. A. Jones, and C. S. Adams, *Cooperative atom-light interaction in a blockaded rydberg ensemble*, *Phys. Rev. Lett.* **105**, 193603 (2010).
- [17] A. V. Gorshkov, J. Otterbach, M. Fleischhauer, T. Pohl, and M. D. Lukin, *Photon-photon interactions via rydberg blockade*, *Phys. Rev. Lett.* **107**, 133602 (2011).
- [18] Y. O. Dudin and A. Kuzmich, *Strongly interacting rydberg excitations of a cold atomic gas*, *Science* **336**, 887 (2012).
- [19] T. Peyronel, O. Firstenberg, Q.-Y. Liang, S. Hofferberth, A. V. Gorshkov, T. Pohl, M. D. Lukin, and V. Vuletic,

---

\* Present address: Department of Physics, Princeton University, Princeton, NJ 08544, USA; mgul-

- Quantum nonlinear optics with single photons enabled by strongly interacting atoms*, Nature **488**, 57 (2012).
- [20] H. Gorniaczyk, C. Tresp, J. Schmidt, H. Fedder, and S. Hofferberth, *Single-photon transistor mediated by interstate Rydberg interactions*, Phys. Rev. Lett. **113**, 053601 (2014).
- [21] D. Tiarks, S. Baur, K. Schneider, S. Dürr, and G. Rempe, *Single-Photon Transistor Using a Förster Resonance*, Phys. Rev. Lett. **113**, 053602 (2014).
- [22] S. Baur, D. Tiarks, G. Rempe, and S. Dürr, *Single-photon switch based on rydberg blockade*, Phys. Rev. Lett. **112**, 073901 (2014).
- [23] D. Tiarks, S. Schmidt, G. Rempe, and S. Dürr, *Optical  $\pi$  phase shift created with a single-photon pulse*, Sci. Adv. **2**, e1600036 (2016).
- [24] J. D. Thompson, T. L. Nicholson, Q.-Y. Liang, S. H. Cantu, A. V. Venkatramani, S. Choi, I. A. Fedorov, D. Viscor, T. Pohl, M. D. Lukin, et al., *Symmetry-protected collisions between strongly interacting photons*, Nature **542**, 206 (2017).
- [25] C. R. Murray and T. Pohl, *Coherent photon manipulation in interacting atomic ensembles*, Phys. Rev. X **7**, 031007 (2017).
- [26] O. Firstenberg, T. Peyronel, Q.-Y. Liang, A. V. Gorshkov, M. D. Lukin, and V. Vuletić, *Attractive photons in a quantum nonlinear medium*, Nature **502**, 71 (2013).
- [27] M. J. Gullans, J. D. Thompson, Y. Wang, Q.-Y. Liang, V. Vuletić, M. D. Lukin, and A. V. Gorshkov, *Effective field theory for rydberg polaritons*, Phys. Rev. Lett. **117**, 113601 (2016).
- [28] K. Jachymski, P. Bienias, and H. P. Büchler, *Three-body interaction of rydberg slow-light polaritons*, Phys. Rev. Lett. **117**, 053601 (2016).
- [29] Q.-Y. Liang, A. V. Venkatramani, S. H. Cantu, T. L. Nicholson, M. J. Gullans, A. V. Gorshkov, J. D. Thompson, C. Chin, M. D. Lukin, and V. Vuletić, *Observation of three-photon bound states in a quantum nonlinear medium*, arXiv:1709.01478 (2017).
- [30] M. J. Gullans and A. V. Gorshkov, in preparation.
- [31] T. Pohl, E. Demler, and M. D. Lukin, *Dynamical crystallization in the dipole blockade of ultracold atoms*, Phys. Rev. Lett. **104**, 043002 (2010).
- [32] J. Otterbach, M. Moos, D. Muth, and M. Fleischhauer, *Wigner crystallization of single photons in cold rydberg ensembles*, Phys. Rev. Lett. **111**, 113001 (2013).
- [33] A. V. Gorshkov, R. Nath, and T. Pohl, *Dissipative many-body quantum optics in rydberg media*, Phys. Rev. Lett. **110**, 153601 (2013).
- [34] M. F. Maghrebi, N. Y. Yao, M. Hafezi, T. Pohl, O. Firstenberg, and A. V. Gorshkov, *Fractional quantum hall states of rydberg polaritons*, Phys. Rev. A **91**, 033838 (2015).
- [35] M. Moos, M. Höning, R. Unanyan, and M. Fleischhauer, *Many-body physics of Rydberg dark-state polaritons in the strongly interacting regime*, Phys. Rev. A **92**, 053846 (2015).
- [36] A. Sommer, H. P. Büchler, and J. Simon, *Quantum Crystals and Laughlin Droplets of Cavity Rydberg Polaritons*, arXiv:1506.00341 (2015).
- [37] N. Schine, A. Ryou, A. Gromov, A. Sommer, and J. Simon, *Synthetic Landau levels for photons*, Nature **534**, 671 (2016).
- [38] N. Jia, N. Schine, A. Georgakopoulos, A. Ryou, A. Sommer, and J. Simon, *A Strongly Interacting Polaritonic Quantum Dot*, arXiv:1705.07475 (2017).
- [39] E. Zeuthen, M. J. Gullans, M. F. Maghrebi, and A. V. Gorshkov, *Correlated photon dynamics in dissipative rydberg media*, Phys. Rev. Lett. **119**, 043602 (2017).
- [40] J.-W. Pan, Z.-B. Chen, C.-Y. Lu, H. Weinfurter, A. Zeilinger, and M. Żukowski, *Multiphoton entanglement and interferometry*, Rev. Mod. Phys. **84**, 777 (2012).
- [41] M. D. Lukin, M. Fleischhauer, R. Cote, L. M. Duan, D. Jaksch, J. I. Cirac, and P. Zoller, *Dipole blockade and quantum information processing in mesoscopic atomic ensembles*, Phys. Rev. Lett. **87**, 037901 (2001).
- [42] P. Bienias, S. Choi, O. Firstenberg, M. F. Maghrebi, M. Gullans, M. D. Lukin, A. V. Gorshkov, and H. P. Büchler, *Scattering resonances and bound states for strongly interacting Rydberg polaritons*, Phys. Rev. A **90**, 053804 (2014).
- [43] See Supplemental Material for more details on two-body scattering with anisotropic mass, scaling analysis of three-body loss rate, and perturbative treatment of the anisotropic mass.
- [44] J. Wang, J. P. D’Incao, B. D. Esry, and C. H. Greene, *Origin of the three-body parameter universality in efimov physics*, Phys. Rev. Lett. **108**, 263001 (2012).
- [45] P. Naidon, S. Endo, and M. Ueda, *Physical origin of the universal three-body parameter in atomic Efimov physics*, Phys. Rev. A **90**, 022106 (2014).
- [46] P. Naidon, S. Endo, and M. Ueda, *Microscopic origin and universality classes of the efimov three-body parameter*, Phys. Rev. Lett. **112**, 105301 (2014).
- [47] R. H. Dicke, *Coherence in Spontaneous Radiation Processes*, Phys. Rev. **93**, 99 (1954).
- [48] J. L. Bohn, M. Cavagnero, and C. Ticknor, *Quasi-universal dipolar scattering in cold and ultracold gases*, New J. Phys. **11**, 055039 (2009).
- [49] H. R. Sadeghpour, J. L. Bohn, M. J. Cavagnero, B. D. Esry, I. I. Fabrikant, J. H. Macek, and A. R. P. Rau, *Collisions near threshold in atomic and molecular physics*, J. Phys. B: At. Mol. Opt. Phys. **33**, R93 (2000).
- [50] J. P. D’Incao and B. D. Esry, *Manifestations of the efimov effect for three identical bosons*, Phys. Rev. A **72**, 032710 (2005).
- [51] J. Wang, J. P. D’Incao, and C. H. Greene, *Numerical study of three-body recombination for systems with many bound states*, Phys. Rev. A **84**, 052721 (2011).
- [52] Y. Wang, J. P. D’Incao, and C. H. Greene, *Efimov effect for three interacting bosonic dipoles*, Phys. Rev. Lett. **106**, 233201 (2011).
- [53] J. P. D’Incao and B. D. Esry, *Mass dependence of ultracold three-body collision rates*, Phys. Rev. A **73**, 030702 (2006).
- [54] L. K. Shalm, D. R. Hamel, Z. Yan, C. Simon, K. J. Resch, and T. Jennewein, *Three-photon energy-time entanglement*, Nature Phys. **9**, 19 (2013).



# Supplemental Material to the Manuscript: “Efimov States of Strongly Interacting Photons”

## I. TWO-BODY SCATTERING WITH ANISOTROPIC MASS

In this section we compare the scaling of the  $T$ -matrix elements with energy for the higher-partial waves in the two-body problem with an anisotropic mass to the Born approximation.

The Schrödinger equation for the wavefunction of two dark-state polaritons (branch  $\mu = D$ ) with identical anisotropic masses in the rescaled coordinates defined in the main text is

$$-\frac{\tilde{\nabla}^2 \psi}{m} + U(\tilde{r}, \tilde{\theta})\psi = E\psi, \quad (\text{S1})$$

$$U(\tilde{r}, \tilde{\theta}) = -\frac{\alpha/\bar{\chi}[2\epsilon_D(\mathbf{q}_0)]}{1 + \frac{\tilde{r}^6}{r_0^6} \left(1 + \frac{\cos^2 \tilde{\theta} \cos 2\beta}{\sin^2 \beta}\right)^3}, \quad (\text{S2})$$

$$\bar{\chi}(\omega) = \frac{\Delta - \omega/2 - \frac{\Omega^2}{\Delta - \omega}}{\omega(\Delta - \omega/2) + 2\Omega^2}, \quad \alpha \approx |S_D^{\mathbf{q}_0}|^4, \quad (\text{S3})$$

$$|S_\mu^{\mathbf{q}}|^2 = \frac{\Omega^2}{\Omega^2 + \epsilon_\mu(\mathbf{q})^2}, \quad (\text{S4})$$

where  $\mathbf{q}_0$  is the incoming momentum of the two dark-state polaritons and  $S_\mu^{\mathbf{q}}$  is the overlap of the single polariton eigenstate on branch  $\mu$  with momentum  $\mathbf{q}$  with the Rydberg state. Expanding the wavefunction in spherical harmonics and dropping the tildes over the rescaled coordinates

$$\psi = \frac{1}{r} \sum_{\ell, m} Y_{\ell m}(\theta, \phi) f_{\ell m}(r), \quad (\text{S5})$$

we arrive at the radial Schrödinger equation

$$-\frac{f''_{\ell m}}{m} + \frac{\ell(\ell+1)}{mr^2} f_{\ell m} + \sum_{\ell'} U_{\ell\ell'}^{(m)}(r) f_{\ell'm} = E f_{\ell m}, \quad (\text{S6})$$

$$U_{\ell\ell'}^{(m)}(r) = 2\pi \int_0^\pi \sin\theta d\theta Y_{\ell m}^*(\theta, \phi) U(r, \theta) Y_{\ell' m}(\theta, \phi), \quad (\text{S7})$$

with the boundary conditions [S1]

$$\lim_{r \rightarrow 0} f_{\ell m}^{\ell' m}(r) = 0, \quad (\text{S8})$$

$$\lim_{r \rightarrow \infty} f_{\ell m}^{\ell' m}(r) = \delta_{\ell\ell'} e^{-i(kr - \frac{\ell'\pi}{2})} - S_{\ell\ell'}^{(m)} e^{i(kr - \frac{\ell'\pi}{2})}. \quad (\text{S9})$$

Here  $k = \sqrt{mE}$  and  $S_{\ell\ell'}^{(m)}$  is the multi-channel  $S$ -matrix, which has to be found self-consistently.

In the first Born approximation the scattering amplitude defined in Eq. (9) of the main text takes the form

$$f(\hat{k}_i, \hat{k}_f) = -\frac{1}{2\pi} \int d^3r e^{i\mathbf{k}_i \cdot \mathbf{r}} U(r, \theta) e^{-i\mathbf{k}_f \cdot \mathbf{r}}. \quad (\text{S10})$$

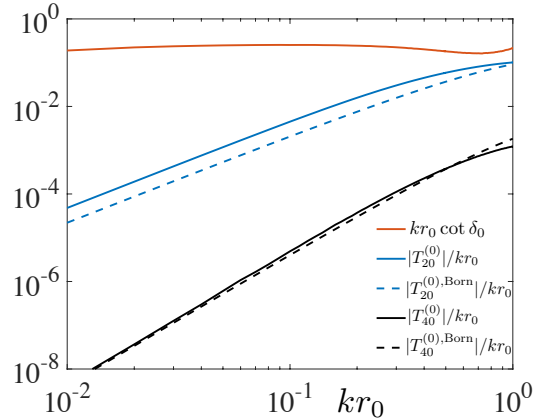


FIG. S1: (a) Scaling of  $T$ -matrix elements as a function of  $k = \sqrt{mE}$ . Near threshold, the scattering is dominated by the diagonal  $s$ -wave component  $S_{00}^{(0)} = e^{i\delta_0(k)}$ , which defines the scattering length via  $k \cot \delta_0 = -1/a + O(k^2)$ . Here we took  $\sqrt{mU(0)}r_0 = 2.2$  and  $m_\perp/m_z = 20$ .

Using the expansion of  $e^{i\mathbf{k} \cdot \mathbf{r}}$  into spherical harmonics, this equation directly implies that

$$T_{\ell\ell'}^{(m), \text{Born}} = -k\Gamma_{\ell\ell'}^{(m)}, \quad (\text{S11})$$

$$\Gamma_{\ell\ell'}^{(m)} = -4 \int r^2 dr j_\ell(kr) j_{\ell'}(kr) U_{\ell\ell'}^{(m)}(r), \quad (\text{S12})$$

where  $j_\ell(x)$  are spherical Bessel functions. For an interaction potential that dies off as  $1/r^s$ ,  $T_{\ell\ell'}^{(m), \text{Born}}$  has the scaling given in Eq. (10) of the main text. We have verified these scalings for the higher partial wave  $S$ -matrix elements using numerical solutions of the radial Schrödinger equation. An example is shown in Fig. S1(a) for the  $s$ -wave channel with a large mass ratio of  $m_\perp/m_z = 20$ . In Fig. 2(c) of the main text we obtained the scattering length through numerical solutions of the  $S$ -matrix including the  $\ell = 0$  and  $\ell = 2$  partial wave channels. We further verified that including the  $\ell = 4$  channel had a negligible effect on the position of the  $s$ -wave scattering resonances, which is consistent with the perturbative analysis in Sec. III.

## II. SCALING OF THREE-BODY LOSS RATE

In this section, we derive the scaling of the three-body loss rate near the EIT resonance for large values of the interaction parameter  $\phi = g^2 r_b / c\Delta = \text{OD}_b \gamma / \Delta$ , where  $\text{OD}_b$  is the optical depth per blockade radius.

From the optical theorem, the three-body loss appears as an imaginary contribution to the self-energy

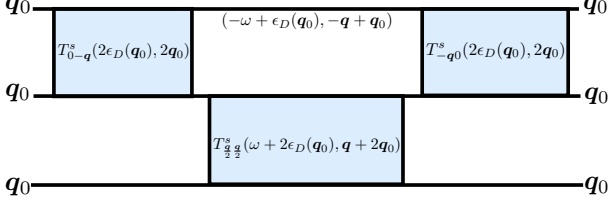


FIG. S2: One-loop contribution to the three-body  $T$ -matrix with all incoming and outgoing states dark-state polaritons at the same momentum. The imaginary part of this diagram gives the lowest order contribution to the three-body loss rate.

of three dark-state polaritons [S2]. Thus we can find the lowest order contribution to the three-body loss rate in the two-body  $T$ -matrix by evaluating the imaginary part of the diagram in Fig. S2, which contains a sin-

$$\int \frac{d^3q}{8\pi^3} \sum_{\mu, \nu, \gamma} |S_{\mu}^{q_0-q}|^2 |S_{\nu}^{q_0+q}|^2 |S_{\gamma}^{q_0+q}|^2 \frac{T_{0-q}^s(2\epsilon_D(\mathbf{q}_0), 2\mathbf{q}_0) T_{\frac{q}{2}}^s(3\epsilon_D(\mathbf{q}_0) - \epsilon_{\mu}(\mathbf{q}_0 - \mathbf{q}), 2\mathbf{q}_0 + \mathbf{q}) T_{-q_0}^s(2\epsilon_D(\mathbf{q}_0), 2\mathbf{q}_0) |S_D^{q_0}|^6}{[2\epsilon_D(\mathbf{q}_0) - \epsilon_{\mu}(\mathbf{q}_0 - \mathbf{q}) - \epsilon_{\nu}(\mathbf{q}_0 + \mathbf{q})][2\epsilon_D(\mathbf{q}_0) - \epsilon_{\mu}(\mathbf{q}_0 - \mathbf{q}) - \epsilon_{\gamma}(\mathbf{q}_0 + \mathbf{q})]}.$$
 (S14)

Neglecting the contribution from two-body poles, which were shown to be strongly suppressed in this system [S3], the only genuine three-body poles in the integrand appear in  $T_{\frac{q}{2}}^s(3\epsilon_D(\mathbf{q}_0) - \epsilon_{\mu}(\mathbf{q}_0 - \mathbf{q}), 2\mathbf{q}_0 + \mathbf{q})$ . When there are deep two-body bound states, the pole will appear at low virtual momentum. Evaluating the integral over this pole will give the lowest order contribution to the three-body recombination rate. In the absence of two-body bound states, the only poles in  $T_{\frac{q}{2}}^s(3\epsilon_D(\mathbf{q}_0) - \epsilon_{\mu}(\mathbf{q}_0 - \mathbf{q}), 2\mathbf{q}_0 + \mathbf{q})$  arise from the kinematically allowed loss processes into free polaritons discussed in the main text, which occur at large  $q_z$ .

To more explicitly demonstrate the exponential suppression of these contributions we note that the two-body  $T$ -matrix can be found from the Lippmann-Schwinger equation for Rydberg polaritons generalized to include the transverse momentum [S3]

$$T_{\mathbf{k}\mathbf{k}'}(\omega, \mathbf{K}) = V_{\mathbf{k}-\mathbf{k}'} + \int \frac{d^3q}{(2\pi)^3} V_{\mathbf{k}-\mathbf{q}} g_{ss}^{\mathbf{q}}(\omega, \mathbf{K}) T_{\mathbf{q}\mathbf{k}'}(\omega, \mathbf{K}),$$
 (S15)

$$g_{ss}^{\mathbf{q}}(\omega, \mathbf{K}) = \sum_{\mu, \nu} \frac{|S_{\mu}^{\mathbf{K}/2+\mathbf{q}}|^2 |S_{\nu}^{\mathbf{K}/2-\mathbf{q}}|^2}{\omega - \epsilon_{\mu}(\mathbf{K}/2 + \mathbf{q}) - \epsilon_{\nu}(\mathbf{K}/2 - \mathbf{q}) + i\epsilon},$$
 (S16)

where  $g_{ss}^{\mathbf{q}}(\omega, \mathbf{K})$  is the non-interacting, time-ordered Green's function for two Rydberg states.

gle loop. In this diagram the shaded boxes represent the symmetrized two-particle  $T$ -matrix  $T_{\mathbf{k}\mathbf{k}'}^s(\omega, K) = [T_{\mathbf{k}\mathbf{k}'}(\omega, \mathbf{K}) + T_{\mathbf{k}-\mathbf{k}'}(\omega, \mathbf{K})]/2$ , where  $\omega$  and  $\mathbf{K} = \mathbf{q}_1 + \mathbf{q}_2$  are the total energy and momentum of the incoming polaritons with momenta  $\mathbf{q}_{1,2}$ , respectively,  $\mathbf{k} = (\mathbf{q}_1 - \mathbf{q}_2)/2$  is the incoming relative momentum of the two polaritons, and  $\mathbf{k}'$  is the outgoing relative momentum. The solid lines are the time-ordered, non-interacting Green's function for a single Rydberg state

$$g_s^{\mathbf{q}}(\omega) = \sum_{\mu} \frac{|S_{\mu}^{\mathbf{q}}|^2}{\omega - \epsilon_{\mu}(\mathbf{q}) + i\epsilon},$$
 (S13)

where  $S_{\mu}^{\mathbf{q}}$  is the overlap of the single polariton eigenstate on branch  $\mu$  with momentum  $\mathbf{q}$  with the Rydberg state. Using these Feynman rules and performing the integral over the virtual frequency  $\omega$ , the diagram in Fig. S2 evaluates to

For relative momenta  $q_z$  much larger than  $g^2/c\Delta$ ,  $g_{ss}^{\mathbf{q}}(\omega, \mathbf{K})$  saturates to the constant

$$\bar{\chi}(\omega) = \lim_{|q_z| \rightarrow \infty} g_{ss}^{\mathbf{q}}(\omega, \mathbf{K})$$
 (S17)

which implies that the  $T$ -matrix for large longitudinal momentum transfers approaches  $T_{\mathbf{k}\mathbf{k}'}(\omega, \mathbf{K}) \approx U_{\mathbf{k}-\mathbf{k}'}/\alpha$ , where  $U_{\mathbf{k}} = \int d^3r e^{i\mathbf{k}\cdot\mathbf{r}} U(\mathbf{r})$  and  $U(\mathbf{r})$  is defined in Eq. (1) of the main text.

From the expressions for  $v_g$  and  $m_{z,\perp}$  in the main text (Eqs. (4)-(6)) we see that near the EIT resonance (i.e.,  $\epsilon_{\mu}(\mathbf{q}) \ll \Delta$ ) and in the regime  $g \gg |\Delta|$  with  $|\Delta| \gg \Omega$ , the typical variations in the dispersion with respect to  $q_z$  occur on momentum scales  $g^2/c\Delta$ . This implies that, in the large  $\phi = g^2 r_b / c\Delta$  limit,  $r_b^{-1}$  is a small momentum scale with respect to the polariton dispersion. From the analysis in the main text we know that, in the absence of two-body bound states, the three-body resonances in Eq. (S14) are associated with large virtual momentum  $q_z$ . This implies that the three-body loss will be exponentially suppressed by the term  $[T_{0\mathbf{q}}^s(2\epsilon_D(\mathbf{q}_0), 2\mathbf{q}_0)]^2 \approx |U_{\mathbf{q}}|^2/\alpha^2$  evaluated at the resonant values of  $\mathbf{q}$ . Near the inflection point there is an additional suppression of the three-body loss from the overlap factor with the incoming and outgoing dark-state polaritons  $|S_D^{q_0}|^6 \approx \Omega^2/\Delta^2$ .



### III. PERTURBATIVE INCLUSION OF MASS ANISOTROPY

In this section, we introduce an approximation method that includes the effect of the anisotropic mass by treating the coupling to the higher-partial waves in the rescaled coordinates perturbatively.

In the rescaled coordinates, the multichannel potential matrix  $U_{\ell\ell'}(r)$  [see Eq. (S6)] fully describes anisotropic interactions on the two-body level. In principle, a numerically exact treatment of the three-body scattering problem requires this multichannel two-body potential, including all partial waves. However, we can most simply describe the qualitative affect of anisotropic interactions on important three-body physics, like the Efimov effect, using a single-channel two-body potential. To this end we use a two-body model potential  $U'(r)$  that perturbatively includes the affect of anisotropic interactions.

For isotropic interactions the potential matrix  $U_{\ell\ell'}(r)$  becomes diagonal, and we can fully describe low-energy scattering using only the  $s$ -wave ( $\ell = 0$ ) potential. We find corrections to this potential due to anisotropic interactions using second-order perturbation theory in an approximation that only captures  $s$ -wave resonances [S1],

$$U'(r) = U_{00}(r) - \sum_{\ell \neq 0}^{\ell_{\max}} \frac{U_{0\ell}^2(r)}{U_{\ell\ell}(r) - U_{00}(r)}, \quad (\text{S18})$$

where the value  $\ell_{\max}$  identifies the highest partial wave included in the model potential  $U'(r)$ . This potential can be numerically converged by taking the limit  $\ell_{\max} \rightarrow \infty$ .

The terms of the sum on the right hand side of equation (S18) decrease rapidly with increasing  $l$ . We define each term as

$$\Delta U'_\ell(r) = -\frac{U_{0\ell}^2(r)}{U_{\ell\ell}(r) - U_{00}(r)}. \quad (\text{S19})$$

We show each non-zero term from  $\ell = 0 - 6$  in Fig. S3, where only even partial waves couple to the  $s$ -wave channel. For  $\ell > 6$  each term is essentially zero for all  $r$  on this scale.

In order to study Efimov physics we tune the depth of our model potential  $U'(0)$  such that a two-body bound state resides at zero energy and the scattering length of this potential diverges. For each choice of  $\ell_{\max}$  this resonant depth is slightly different. Table I shows these

depths for a mass ratio  $m_\perp/m_z = 10$ . We see that the depth converges quickly as a function of  $\ell_{\max}$  and that the addition of  $\Delta U'_6(r)$  makes less than a 0.1% change in the depth. Therefore, we neglect contributions to  $U'(r)$  from channels of partial-wave character greater than  $\ell = 6$ . Furthermore, the position of the first scattering resonance computed using this approximation agrees with the non-perturbative calculations presented in Fig. 2(c) of the main text and in Sec. I. We choose  $\ell_{\max} = 6$  to construct the model potential  $U'(r)$ , and we compute three-body potentials using this model. Although an accurate description of the three-body physics requires the

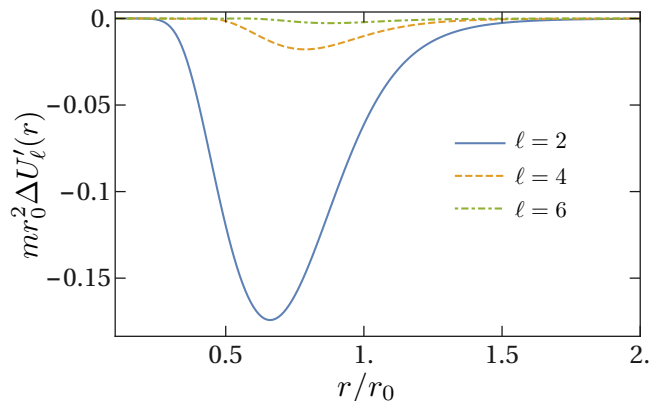


FIG. S3: Each non-zero term  $\Delta U'_\ell(r)$  in the perturbative correction to the potential  $U_{00}(r)$  due to anisotropic interactions. We show the range  $\ell = 0 - 6$ . The mass ratio  $m_\perp/m_z = 10$ .

full treatment of the anisotropic character of the two-body interactions, our simple model is able to qualitatively describe the dependence of Efimov physics on the strength of the anisotropy (see, for instance, Ref. [S4])

TABLE I: The depth of the potential  $U'(r)$  that supports a zero-energy bound state, for each value of  $\ell_{\max}$ . The mass ratio  $m_\perp/m_z = 10$ .

$\ell_{\max}$	$\sqrt{-mU'(0)}r_0$
0	2.3339
2	2.2705
4	2.2645
6	2.2635

[S1] J. L. Bohn, M. Cavagnero, and C. Ticknor, *Quasi-universal dipolar scattering in cold and ultracold gases*, New J. Phys. **11**, 055039 (2009).

[S2] E. Braaten and H. W. Hammer, *Three-Body Recombination into Deep Bound States in a Bose Gas with Large Scattering Length*, Phys. Rev. Lett. **87**, 160407 (2001).

[S3] P. Bienias, S. Choi, O. Firstenberg, M. F. Maghrebi, M. Gullans, M. D. Lukin, A. V. Gorshkov, and H. P.

Büchler, *Scattering resonances and bound states for strongly interacting Rydberg polaritons*, Phys. Rev. A **90**, 053804 (2014).

[S4] Y. Wang, J. P. D’Incao, and C. H. Greene, *Efimov effect for three interacting bosonic dipoles*, Phys. Rev. Lett. **106**, 233201 (2011).